Extending Multiresolution Time-Domain (MRTD) Technique to the Simulation of High-Frequency Active Devices

Yasser A. Hussein and Samir M. El-Ghazaly, *Fellow, IEEE*

***Abstract*—We present a new time-domain simulation approach for large-signal physical modeling of high-frequency semiconductor devices using wavelets. The proposed approach solves the complete hydrodynamic model, which describes the transport physics, on nonuniform self-adaptive grids. The nonuniform grids are obtained by applying wavelet transforms followed by hard thresholding. This allows forming fine and coarse grids in locations where variable solutions change rapidly and slowly, respectively. A general criterion is mathematically defined for grid updating within the simulation. In addition, an efficient thresholding formula is proposed and verified. The developed technique is validated by simulating a submicrometer FET. Different numerical examples are presented along with illustrative comparison graphs, showing over 75% reduction in CPU time, while maintaining the same degree of accuracy achieved using a uniform grid case. Tradeoffs between threshold values, CPU time, and accuracy are discussed. To our knowledge, this is the first time in the literature to implement and report a wavelet-based hydrodynamic model simulator. This study also represents a fundamental step toward applying wavelets to Maxwell's equations in conjunction with the hydrodynamic model for accurate modeling of high-frequency active devices aiming to reduce the simulation time, while maintaining the same degree of accuracy.**

***Index Terms*—Adaptive grids, biorthogonal wavelets, full hydrodynamic model, global modeling, multiresolution time domain (MRTD), semiconductor simulation.**

I. Introduction

MODERN high-performance electronics are based on technologies such as monolithic microwave integrated circuits (MMICs), with a large number of closely packed passive and active structures, and several levels of transmission lines and discontinuities. These devices operate at high speeds, frequencies, and often over very broad bandwidths. It is thus perceptible that the design of MMICs should be based on robust design tools that would simulate all circuit elements simultaneously. The possibility of achieving this type of modeling is addressed by global circuit modeling that has been demonstrated in [1]–[6].

Manuscript received November 6, 2002; revised February 16, 2003. This work was supported by the Army Research Office under Contract DAAD-19-99-1-0194.

Y. A. Hussein is with the Telecommunication Research Center, Arizona State University, Tempe, AZ 85287 USA (e-mail: yasser.hussein@asu.edu).

S. M. El-Ghazaly is with the Department of Electrical and Computer Engineering, University of Tennessee, Knoxville, TN 37996 USA (e-mail: el-ghazaly@utk.edu).

Digital Object Identifier 10.1109/TMTT.2003.814315

Global modeling is a tremendous task that involves advanced numerical techniques and different algorithms. As a result, it is computationally expensive [6]. Therefore, there is an urgent need to present a new approach to reduce the simulation time, while maintaining the same degree of accuracy presented by global modeling techniques. One approach is to adaptively refine grids in locations where the unknown variables vary rapidly. Such a technique is called multiresolution time domain (MRTD), and a very attractive way to implement it is to use wavelets [7], [8].

The MRTD approach has been successfully applied to finite-difference time-domain (FDTD) simulations of passive structures [9]–[20]. However, for the active devices, which are characterized by a set of coupled and highly nonlinear partial differential equations (PDEs), applying the same approach would become quite time consuming [21]. Several different approaches for solving PDEs using wavelets have been considered. It has been observed by several authors that nonlinear operators such as multiplication are too computationally expensive when conducted directly on a wavelet basis. One of the approaches for solving PDEs is the interpolating wavelets technique presented in [22], in which the nonlinearities are dealt with using the so-called sparse point representation (SPR). Interpolating wavelets have been successfully applied to the simple drift-diffusion active device model [23]–[25]. Being primarily developed for long-gate devices, the drift-diffusion model leads to inaccurate estimations of device internal distributions and microwave characteristics for submicrometer devices [26]. It is worth mentioning that, in [22], the author proposed a new technique to solve simple forms of hyperbolic PDEs using an interpolating wavelet scheme. These PDEs can represent Maxwell's equations or the simple drift-diffusion model, but not the complete hydrodynamic model. Thus, a new approach to apply wavelets to the hydrodynamic model PDEs is needed for accurate modeling of submicrometer devices, while achieving a CPU time reduction.

In this paper, a new approach to apply wavelets to the full hydrodynamic model is developed and employed in a two-dimensional (2-D) large-signal simulator. The main idea is to take snap shots of the solution during the simulation and apply biorthogonal wavelet transform to the current solution to obtain the coefficients of the details. The coefficients of the details are then normalized, and a threshold is applied to obtain a nonuniform grid. A general grid-updating criterion, as well as a threshold formula, have been developed and verified. In addition, problems that are related to boundary conditions and discritization

are carefully addressed and solved. The complete description of the proposed approach is provided. Furthermore, a comprehensive set of results is included along with illustrative comparison graphs.

This paper is organized as follows. Section II reviews briefly the theory of the MRTD. Problem description is given in Section III. Full descriptions of the proposed algorithm along with illustrative graphs are provided in Section IV. Results and discussions are presented in Section V. Error and stability analysis are discussed in Section VI. Finally, conclusions are provided in Section VII.

II. Fundamentals of the MRTD

The construction of biorthogonal wavelet bases relies on the notation of multiresolution analysis [27]. This notation gives a formal description of the intuitive idea that every signal can be constructed by a successive refinement by iteratively adding *details* to an *approximation*. The coefficients of the approximations are given by

$$a_x[n,m] = \int_{-\infty}^{+\infty} x(t)\varphi_{nm}(t)dt \tag{1}$$

where $\varphi_{nm}(t)$ is the family of dilates and translates of the scaling function formed as

$$\varphi_{nm}(t) = 2^{(m/2)}\varphi(2^m t - n). \tag{2}$$

On the other hand, (3) gives the coefficients of the details as follows:

$$d_x[n,m] = \int_{-\infty}^{+\infty} x(t)\psi_{nm}(t)dt \tag{3}$$

where $\psi_{nm}(t)$ is the family of dilates and translates of the wavelet function defined as

$$\left\{\psi_{nm}(t) = 2^{(m/2)}\psi(2^m t - n), \qquad n,m \in Z\right\}. \tag{4}$$

While some wavelets such as Daubechies are asymmetrical [27], it is possible to create symmetric wavelets with compact support by using two sets of wavelets: one to compose the signal and the other to construct it. Such wavelets are called *biorthogonal* [28].

III. Problem Description

The transistor model used in this study is a 2-D full-hydrodynamic large-signal physical model. The active device model is based on the moments of Boltzmann's transport equation, obtained by integrating over the momentum space. The integration results in a strongly coupled highly nonlinear set of PDEs, called the conservation equations. These equations provide a time-dependent self-consistent solution for carrier density, carrier energy, and carrier momentum, which are given as follows.

- *Current continuity*

$$\frac{\partial n}{\partial t} + \nabla \cdot (n\upsilon) = 0. \tag{5}$$

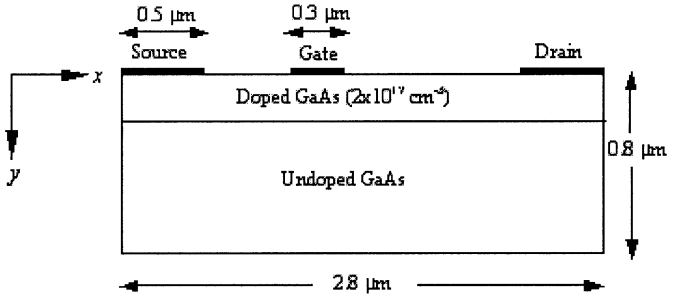

Fig. 1. Cross section of the simulated transistor.

- *Energy conservation*

$$\frac{\partial(n\varepsilon)}{\partial t} + qn\upsilon \cdot \boldsymbol{E} + \nabla \cdot \left(n\upsilon(\varepsilon + K_B T)\right) = -\frac{n(\varepsilon - \varepsilon_0)}{\tau_\varepsilon(\varepsilon)}. \tag{6}$$

- *x-momentum conservation*

$$\frac{\partial(np_x)}{\partial t} + qnE_x + \frac{\partial}{\partial x}(np_x\upsilon_x + nK_B T) = -\frac{n(p_x - p_0)}{\tau_m(\varepsilon)}. \tag{7}$$

In the above equations, n is the electron concentration, υ is the electron velocity, $\boldsymbol{E}$ is the electric field, ε is the electron energy, ε_0 is the equilibrium thermal energy, and p is the electron momentum. The energy and momentum relaxation times are given by τ_ε and τ_m, respectively. Similar expression can be obtained for the y-direction momentum. The three conservation equations are solved in conjunction with Poisson's equation

$$\nabla^2\varphi = \frac{q}{\in}(N_d - n) \tag{8}$$

where φ is the electrostatic potential, q is the electron charge, $\in$ is the dielectric constant, N_d is the doping concentration, and n is the carrier concentration at any given time. The total current density distribution $\boldsymbol{J}$ inside the active device at any time t is given as

$$\boldsymbol{J}(t) = -qn\upsilon(t). \tag{9}$$

The low field mobility is given by the empirical relation [29]

$$\mu_0 = \frac{8000}{1 + (N_d \cdot 10^{-17})^{0.5}} \frac{\text{cm}^2}{\text{V} \cdot \text{s}.} \tag{10}$$

The above model accurately describes all the nonstationary transport effects by incorporating energy dependence into all the transport parameters such as effective mass and relaxation times. Fig. 1 shows the cross section of the simulated structure with parameters summarized in Table I.

Next, we will demonstrate that wavelets can be applied to the full hydrodynamic simulator to accurately model submicrometer gate devices with significantly less CPU time. Ultimately, a full hydrodynamic model should be implemented with Maxwell's equations rather than Poisson's equation to obtain a self-consistent simulation of electromagnetic-wave propagation effects.

TABLE I
TRANSISTOR PARAMETERS USED IN THE SIMULATION

Drain and source contacts	0.5 μm
Gate-source separation	0.5 μm
Gate-drain separation	1.0 μm
Device thickness	0.8 μm
Device length	2.8 μm
Gate length	0.3 μm
Device Width	200 μm
Active layer thickness	0.2 μm
Active layer doping	$2\text{x}10^{17}$ cm^{-3}
Schottky barrier height	0.8 V
DC gate-source voltage	-0.5 V
DC drain-source voltage	3.0 V

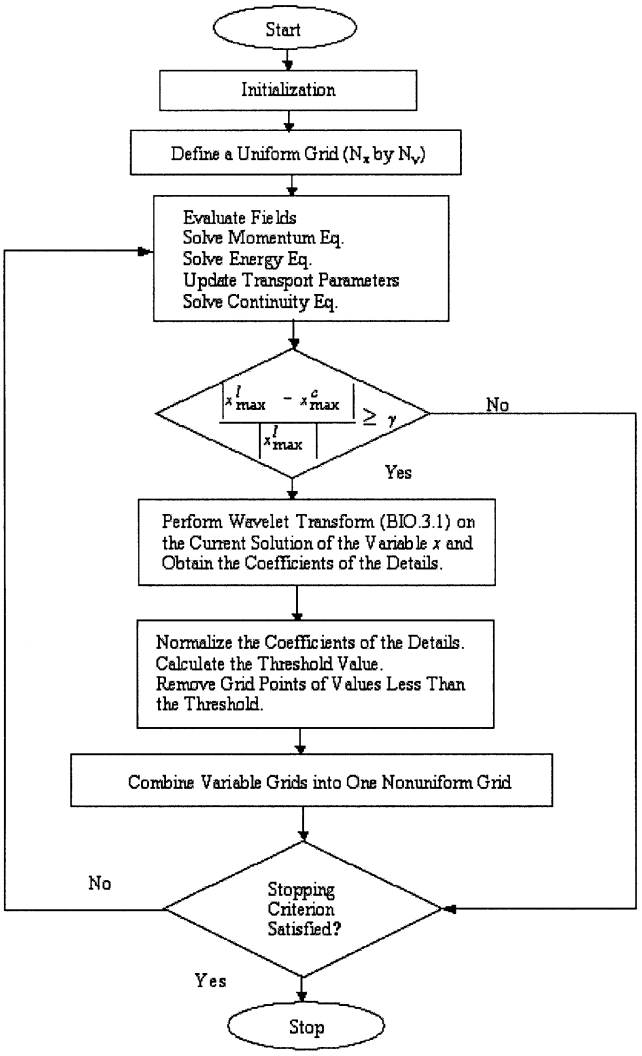

Fig. 2. Generic flowchart of the proposed algorithm.

IV. PROPOSED ALGORITHM

Fig. 2 shows the flowchart of the proposed algorithm. A uniform grid is defined at the beginning of the simulation. Equations (5)–(9) are then solved in the sequence shown in the flowchart to update the grid of the different variables at the new iteration with the following criterion:

$$\frac{\left|x^{l}_{\max,\min} - x^{c}_{\max,\min}\right|}{\left|x^{l}_{\max,\min}\right|}. \tag{11}$$

The updating criterion checks if the solution of the variable x has changed by γ since the last iteration using a wavelet transform. The subscripts c and l designate quantities defined in the current time and last time where the wavelet transform is performed, respectively. The subscript $\max, \min$ indicates that the maximum and minimum of the variable x are checked with (11) at the same time. It is worth mentioning here that boundary grid points are not included for the maximum or minimum checking. The value of γ used in the simulation is 0.1. If (11) is satisfied, a wavelet transform is performed on the current variable solution followed by thresholding to obtain a new nonuniform grid for the variable x. Biorthogonal wavelets are used with notation BIO3.1 to point out three vanishing moments for the mother wavelet and only one vanishing moment for the scaling function. The nonuniform grids of the different variables are then combined into only one nonuniform grid for the next iteration. The above steps are repeated until the stopping criterion is satisfied.

It should be noted that magnitude ranges of the variables used in the simulations vary dramatically. For instance, carrier density per cm^{-3} is on the order of 10^{17}, while energy expressed in electronvolts is on the order of 0.5. Accordingly, the threshold value should be dependent on the variable solution at any given iteration. The proposed threshold formula is given by (12) as follows:

$$T = T_0 n_x^{-1} \left(\sum_{i=1}^{n_x} d_i^2 \right)^{0.5}. \tag{12}$$

In this equation, T_0 is the initial threshold value, d_i's are the coefficients of the details, and n_x is the number of grid points in the x-direction. Hence, the value of the threshold depends mainly on the variable solution at any given time rather than being fixed. The values of T_0 used in the simulation are 0.001, 0.01, and 0.05, respectively.

In this paper, a new technique to conceive the nonuniform grids using wavelets has been developed. The main idea is to apply a wavelet transform to the variable solution at any given time to obtain the coefficients of the details, which are then normalized to its maximum. Only grid points where the value of the normalized coefficients of the details larger than the threshold value given by (12) are included. Figs. 3 and 4 illustrate different examples of the technique employed to obtain the nonuniform grids for the electron energy and x-momentum solutions at a particular cross section. Fig. 3 exemplifies how the proposed algorithm obtains the nonuniform grid using transverse compression only. For instance, Fig. 3(a) shows the normalized amplitude of the coefficients of the details for the electron energy, while Fig. 3(b) marks the grid points remaining after thresholding the normalized coefficients of the details using (12). It should be observed that the proposed technique accurately removes grid points in the locations where variable solutions change very slowly.

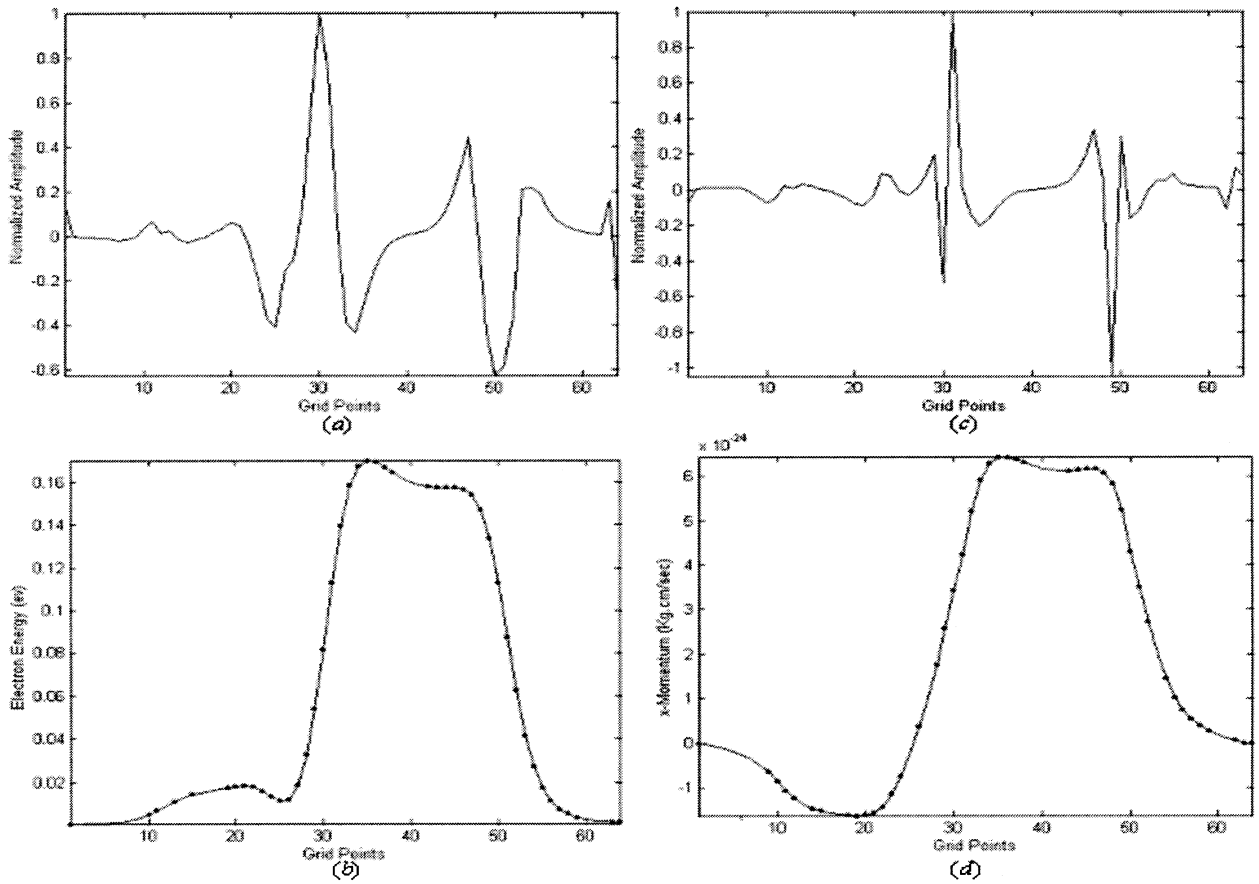

Fig. 3. (a) Normalized details coefficients for the electron energy at a certain transverse cross section. (b) Grid points marked on the actual curve for the electron energy at the same transverse cross section. (c) Normalized details coefficients for the x momentum at a certain transverse cross section. (d) Grid points marked on the actual curve for the x momentum at the same transverse cross section.

Fig. 4 shows the method adopted to obtain the nonuniform grid using longitudinal compression only. Considering Figs. 3 and 4, one can conclude that the compression in the longitudinal cross sections is much more than that in the transverse cross sections. This is consistent with the fact that the physical changes in longitudinal cross sections are much slower compared to those in transverse cross sections.

Fig. 5 shows the procedure employed to obtain the nonuniform grid of the electron energy. The process is achieved by obtaining two separate grids for the transverse and longitudinal compressions, respectively. The two grids are then combined together using logical "AND" to conceive the overall grid for the electron energy at this given time. The same process is conducted for the other variables including x momentum, y momentum, carrier density, and potential whenever (11) is satisfied. The separate grids of our variables are then combined using logical "OR" to obtain the overall grid for the next iteration.

The overall grid obtained needs further processing in order to define a finite-difference (FD) scheme on it. The simplest way to achieve that is to have the same number of grid points for the parallel cross sections, while the number of grid points in the longitudinal cross sections and the transverse cross sections need not be the same. Considering the overall grid given by Fig. 5(d), the number of unknowns remaining after adding the necessary grid points is approximately 35%, which shows that the proposed approach has achieved a reduction in the number of unknown despite of the overhead introduced by adding the extra grid points. Following the above procedure, it was found that boundary conditions implementation, including ohmic and Schottky contacts, does not need special treatment. They can be treated similar to the standard FD scheme. The only issue the algorithm needs to keep track of is identifying the new boundaries of the metallic contacts for each new grid, which is straightforward.

Table II shows the evolution of the nonuniform grids. It can be observed that the number of grid points for the overall grid increases as time advances. The reason is that, at the beginning of the simulation, the solution is not completely formed yet. As the time marches, more grid points are needed to incorporate the changes in the solution. Furthermore, the different variable grids should not be updated at the same rate. For instance, it is apparent that the potential grid needs not to be updated at the same rate as the other variables. Notice that Table II is used for illustration purposes to demonstrate the way the different variable grids change. In the actual simulator, the potential grid is updated a few times at the beginning of the simulation, and then it remains unchanged.

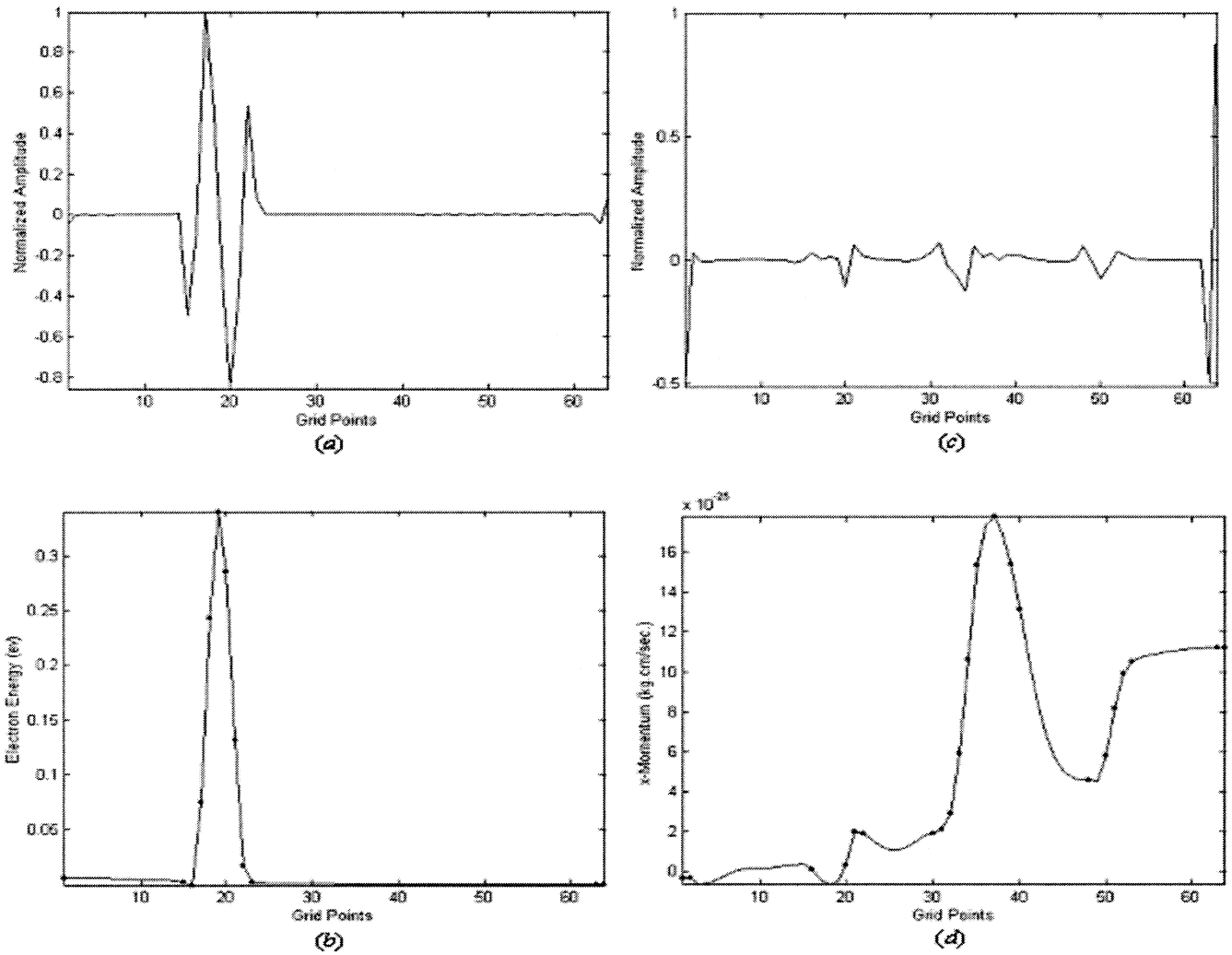

Fig. 4. (a) Normalized details coefficients for the electron energy at a certain longitudinal cross section. (b) Grid points marked on the actual curve for the electron energy at the same longitudinal cross section. (c) Normalized details coefficients for the x momentum at a certain longitudinal cross section. (d) Grid points marked on the actual curve for the x omentum at the same longitudinal cross section.

V. Results and Discussions

A. DC Simulation Results

The approach presented in this paper is general and can be applied to any unipolar transistor. To demonstrate the potential of this approach, it is applied to an idealized MESFET structure, which is discretized by a mesh of 64 Δx by 64 Δy with $\Delta t = 0.001\ ps$. Forward Euler is adopted as an explicit FD method. In addition, upwinding is employed to ensure a stable FD scheme. The space-step sizes are adjusted to satisfy Debye length, while the time-step value Δt is chosen to satisfy the Courant–Friedrichs–Levy (CFL) condition. First, dc simulations are performed following the flowchart presented in Fig. 2, and the current density is calculated using (9). DC excitation is performed by forcing the potential to be equal to the applied voltages to the electrodes (i.e., Dirichlet boundary conditions).

Fig. 6 shows the remaining number of unknowns or grid points versus iteration number for different initial threshold values. Notice that, as the threshold value increases, the remaining number of grid points decreases. At the end of the simulation and for an initial threshold value of 0.1%, the remaining number of unknowns is almost 70%, whereas for an initial threshold value of 1%, the remaining number of unknowns is approximately 30%. The remaining number of unknowns is very sensitive to the initial threshold value in a way that small changes in T_0 results in considerable changes in the remaining number of unknowns.

Furthermore, it is observed that the remaining number of unknowns change during the simulation and this is associated with the grid adaptability used in the simulation. In the following section, we will study the effect of the initial threshold value on the final result accuracy as well the tradeoff between accuracy and CPU time.

It is important to note that a suitable approach to investigate the capabilities of the proposed technique is to compare it to the uniform-grid algorithm. In this case, the new simulator will be accurately evaluated since both algorithms, i.e., wavelet-based and uniform, will run on the same computer. In addition, both algorithms will have the same discritization schemes and the exact semiconductor parameters.

Fig. 7 shows the drain–current convergence curves versus CPU time in seconds for the cases of the uniform grid and

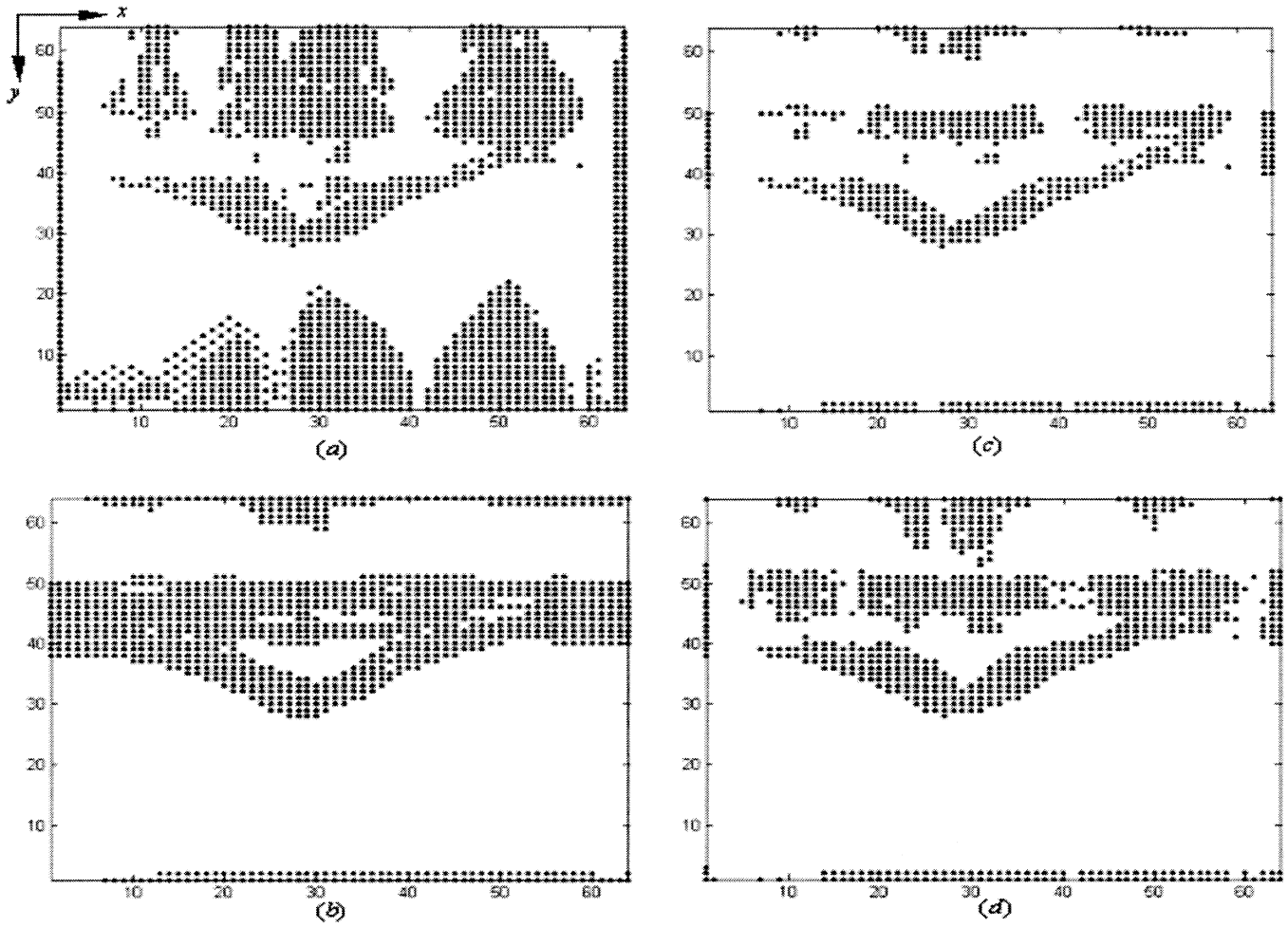

Fig. 5. (a) Compression for the electron energy at the transverse cross sections. (b) Compression for the electron energy at the longitudinal cross sections. (c) Final grid for the electron energy. (d) Overall grid.

the proposed wavelet-based adaptive grids with different initial threshold values T_0. Fig. 7 demonstrates that using the proposed wavelet-based grids approach reduces the CPU time dramatically. For instance, there is a reduction of approximately 75% in CPU time over the uniform grid case for the initial threshold value of 1%, while the dc drain current error is within 1%. In addition, increasing the initial threshold beyond certain value has a negative effect on the accuracy of the final result. This is apparent for T_0 equal to 5%, where there is no agreement between the results achieved using the uniform grid case and the wavelet-based nonuniform grids. The reason is that using large values of T_0 implies that more grid points are removed, including important grid points that will have a negative effect on the final result. On the other hand, using a very small threshold values implies redundant grid points. In summary, there should be an optimal value of T_0 such that both CPU time and error are minimized. In this study, T_0 of 1% is suggested to have a considerable reduction in CPU time, while keeping the error within an acceptable range.

Fig. 8 shows the potential distribution obtained using the proposed algorithm with T_0 equal to 1%. This graph demonstrates that boundary conditions are satisfied at the electrodes. For instance, the value of potential at the gate equals to -1.3 V, which is the applied dc voltage minus the Schottky barrier height.

The values of the elements of the small-signal equivalent-circuit model are computed from the variations in voltages, currents, and charges due to small changes in the dc bias voltages and/or currents. For instance, the small signal gate–source capacitance and transconductance are computed as

$$C_{\rm gs} = \frac{\Delta Q_g}{\Delta V_{\rm gs}} \tag{13}$$

$$g_m = \frac{\Delta I_d}{\Delta V_{\rm gs}} \tag{14}$$

where Q_g is the charge on the gate electrode and $V_{\rm gs}$ is the gate–source voltage. The charge Q_g is calculated using the integral form of Gauss's law. An important figure-of-merit that can be evaluated from these parameters is the device unit-gain cutoff frequency given by (15) as follows:

$$f_t = \frac{g_m}{2\pi C_{\rm gs}}. \tag{15}$$

The values of $C_{\rm gs}$ and g_m are plotted against the applied gate–source voltage for both the uniform-grid case and proposed algorithm. Fig. 9 shows the comparison, where the good agreement between the proposed algorithm and uniform-grid case can be observed. Using the proposed algorithm and for

TABLE II
GRID ADAPTABILITY OF THE DIFFERENT VARIABLES FOR $T_0 = 1\%$

Variable	Unknowns Remaining After Transverse Compression (%)	Unknowns Remaining After Longitudinal Compression (%)	Total Unknowns Remaining (%)
	Time Iteration # 120		
Potential	5.69	7.74	0.63
Carrier Density	6.54	14.92	2.64
Energy	39.65	17.63	8.54
x -Momentum	43.39	16.06	9.18
y -Momentum	16.11	17.53	3.78
All Variables	65.14	22.36	14.43
	Time Iteration # 250		
Potential	5.88	8.59	0.76
Carrier Density	13.69	16.70	5.18
Energy	39.21	23.00	12.26
x -Momentum	43.65	19.09	10.64
y -Momentum	20.02	19.46	7.95
All Variables	61.94	28.93	20.58
	Time Iteration # 480		
Potential	6.27	9.23	0.90
Carrier Density	21.51	17.16	7.71
Energy	43.99	28.88	15.72
x -Momentum	38.57	23.44	12.72
y -Momentum	26.20	26.76	13.53
All Variables	58.84	36.25	25.05
	Time Iteration # 590		
Potential	6.04	9.64	0.93
Carrier Density	29.88	18.24	10.61
Energy	48.85	31.88	18.43
x -Momentum	41.91	29.08	16.21
y -Momentum	32.91	37.04	20.36
All Variables	62.36	44.73	31.74
	Time Iteration # 730		
Potential	7.01	11.13	1.15
Carrier Density	34.08	16.55	8.42
Energy	39.77	35.64	18.43
x -Momentum	41.91	27.98	13.32
y -Momentum	51.46	34.84	25.00
All Variables	62.84	58.96	36.43

$V_{\rm gs} = -0.5$ V, g_m is found to be 263 mS/mm, and $C_{\rm gs}$ is found to be 0.47 pF/mm. In this case, the unit-gain cutoff frequency is calculated using (15) to be 90 GHz.

B. AC Simulation Results

The ac excitation applied to the gate electrode is given as

$$\mathrm{V_{gs}}(t) = \mathrm{V_{gs0}} + \Delta v_{\rm gs} \sin(\omega t) \tag{16}$$

where $V_{\rm gs0}$ is the dc bias applied to the gate electrode, ω is the frequency of the applied signal in radians per second, and $\Delta v_{\rm gs}$ is the peak value of the ac signal (0.1 V). The frequency used in the simulation is 60 GHz. AC excitation is implemented in the same manner as in dc excitation. However, values of the gate potential are obtained at the new time t using (16).

First, the dc solution is obtained by solving Poisson's equation in conjunction with the three hydrodynamic conservation equations. A new value of the gate–source voltage is then calculated using (16). This new value is used to update Poisson's equation for the new voltage distribution and, consequently, the new electric field. The electric field is then used to update the variables in the conservation equations. This process is repeated every Δt following the proposed algorithm given by Fig. 2 until $t = t_{max}$. The current density is obtained using (9). The current density calculated on the plan located midway between the drain and gate is integrated to obtain the total current. The output voltage is estimated by multiplying the total current by the resistance that defines the dc operating point (Q point) of the transistor.

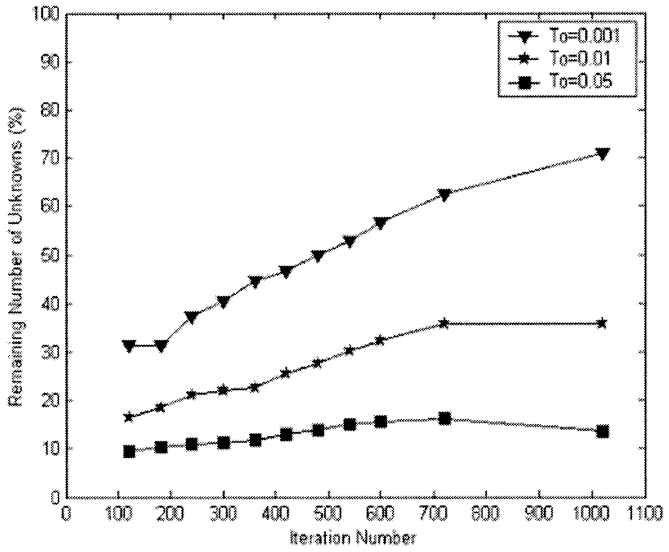

Fig. 6. Remaining number of unknowns as a percentage versus the iteration number for different initial threshold values.

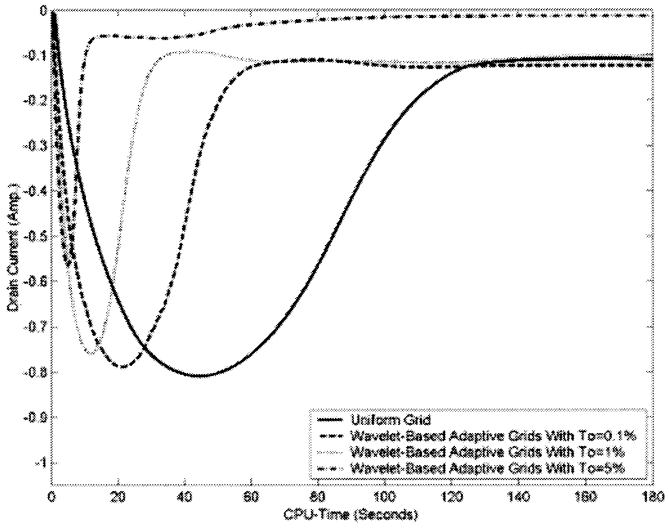

Fig. 7. DC drain–current convergence curves for the uniform grid and the proposed wavelet-based nonuniform grids for different initial threshold values.

Fig. 10 shows the output voltage obtained using the proposed algorithm with $T_0 = 1\%$. A gain of 11 dB is achieved. Moreover, it is observed that there is an output delay of approximately 1 ps that represents the time required for the transistor to respond to the input signal.

Fig. 11 shows the output voltage for the uniform-grid case and the proposed algorithm with different initial threshold values T_0. The purpose of this figure is to emphasize that an optimal value of the threshold should be employed to maintain the required accuracy, while keeping CPU time as minimum as possible. It is observed that using different values of T_0 affects the accuracy of the solution. For instance, using a large value of T_0 results in a completely different solution, and this means the scheme for this special case is inaccurate. This is apparent for the case of T_0 equal to 5% since employing a large value of T_0 results in removing significant grid points, which degrades the final results. Similar to dc simulations, the existence of an optimal

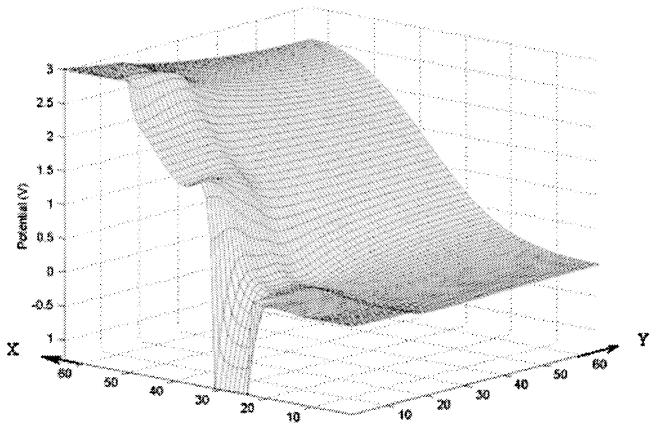

Fig. 8. DC potential distribution obtained by the proposed algorithm using a value of the initial threshold equals to 1%.

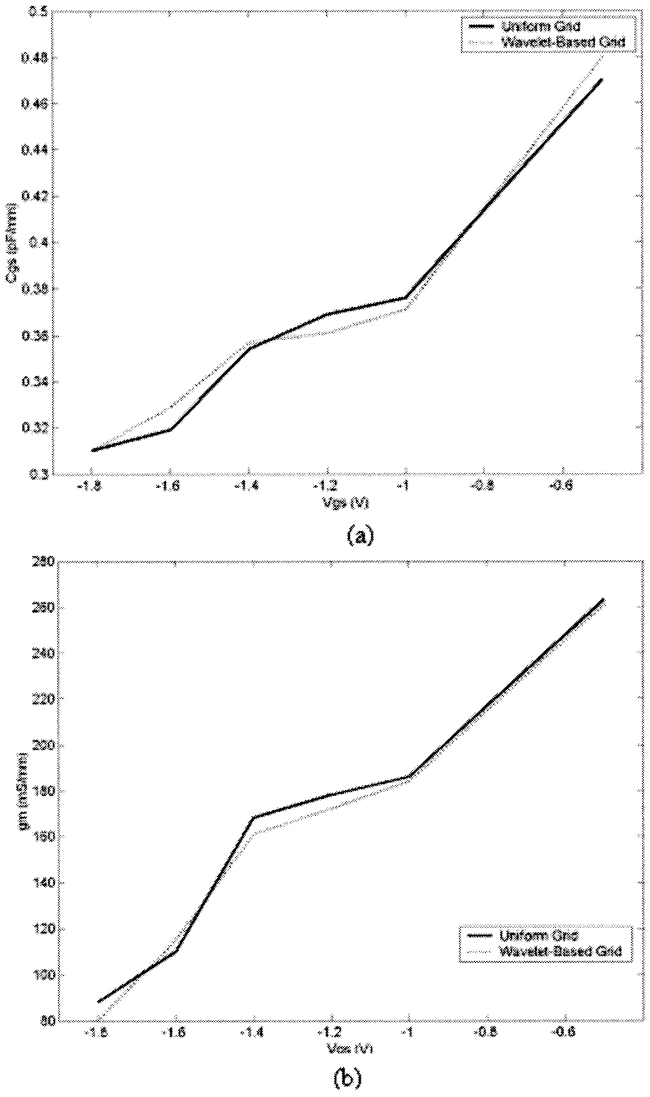

Fig. 9. Comparison between the uniform grid and the proposed algorithm with a value of the initial threshold equals to 1% (a) Gate–source capacitance versus gate–source voltage. (b) Transconductance versus gate–source voltage.

value for T_0 is suggested. Furthermore, it is noticed that there is no significant difference in terms of accuracy between the two cases of $T_0 = 0.1\%$ and $T_0 = 1\%$. The mean relative error

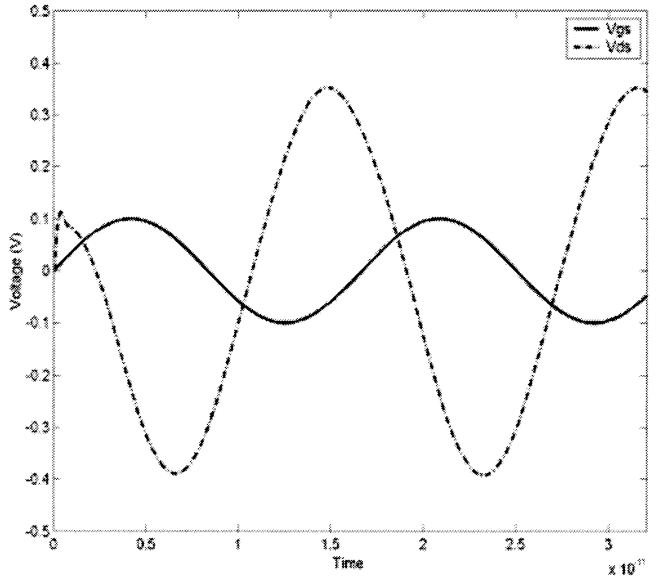

Fig. 10. Large-signal result obtained by the proposed algorithm for a value of the initial threshold equals to 1%.

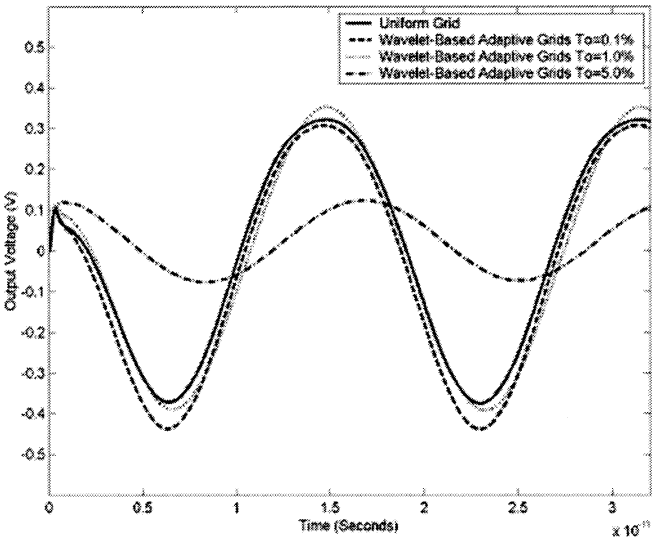

Fig. 11. AC output voltage for the uniform grid and the proposed wavelet-based nonuniform grids with different values of the initial threshold.

obtained for the two cases is in the order of 3%–4%. This suggests that using T_0 equal to 1% is the right choice in terms of both accuracy and CPU time.

VI. Scheme Error and Stability Analysis

It is important to mention here that the simulation and physical times are completely separate entities. The simulation time required to model a specific physical process should vary depending on the technique implemented in the simulation.

The purpose of this section is to demonstrate that the mechanism by which error is introduced when employing the proposed wavelet-based technique is different from the uniform-grid case. The local truncation error for the uniform grid case is dependent, in general, on the mesh spacing (Δx and Δy) and the time step used Δt. On the other hand, the local truncation error for the wavelet-based nonuniform grids approach depends on how accurately the important grid points are reserved, as well as the time step used. This suggests that the local truncation errors, due to spatial discretization, for the uniform grid case and the wavelet-based nonuniform grids are different. The local truncation error accumulates from iteration to iteration. The total truncation or discritization error is thus dependent on the number of iterations used (space and time iterations combined). Accordingly, one can conclude that the total error introduced by the wavelet-based technique due to the local discritization errors accumulating during the simulation may or may not be larger than that of the uniform grid case, at least for the two cases of $T_0 = 0.1\%$ and $T_0 = 1\%$. The reason is that the number of iterations required reaching the steady-state solution for the uniform grid case is much larger than that of the proposed algorithm. In summary, the total error introduced depends on the local truncation error along with the number of iterations required to reach the final solution. This explains the results in the paper comparison figures, where it would be difficult to draw a precise conclusion of which technique is more accurate. This is because for each case or curve, the number of iterations required to obtain the steady-state solution and the local discritization errors are different. The problem of identifying the most accurate solution becomes even more difficult since we are dealing with a highly nonlinear problem.

It is worth mentioning here that the proposed algorithm does not have any stability constraints if Δt is chosen to satisfy the CFL condition at the beginning of the simulation. The reason is, as the simulation progresses, the spatial distances employed become even larger than the ones introduced at the beginning. This represents an extra benefit of using the proposed algorithm in that it does not need any time-step Δt change while the simulation is in progress.

VII. Conclusions

A new wavelet approach has been developed and successfully applied to a 2-D full hydrodynamic large-signal simulator. The proposed algorithm solves the highly nonlinear PDEs that characterize the semiconductor device behavior on nonuniform self-adaptive grids. The nonuniform grids are conceived by applying wavelet transforms to the variable solution followed by thresholding. It is found that each variable has its own grid at any given time, and the grids of the different variables need not be updated at the same rate. A reduction of 75% in CPU time is achieved compared to a uniform grid case with an error of 2% on the dc drain current for a 1% initial threshold value. Furthermore, the same CPU-time reduction has been achieved for ac simulations with a mean relative error of order 3%–4%. It has been observed that tradeoffs exist between the threshold value, CPU time, and accuracy, suggesting an optimal value for the threshold. The proposed algorithm efficiently solves both dc and large-signal ac problems.

References

[1] S. El-Ghazaly and T. Itoh, "Electromagnetic interfacing of semiconductor devices and circuits," in *Proc. IEEE MTT-S Int. Microwave Symp. Dig.*, 1997, pp. 151–154.

[2] S. M. S. Imtiaz and S. M. El-Ghazaly, "Global modeling of millimeter-wave circuits: Electromagnetic simulation of amplifiers," *IEEE Trans. Microwave Theory Tech.*, vol. 45, pp. 2208–2216, Dec. 1997.
[3] A. Witzig, C. Schuster, P. Regeli, and W. Fichtner, "Global modeling of microwave applications by combining the FDTD method and a general semiconductor device and circuit simulator," *IEEE Trans. Microwave Theory Tech.*, vol. 47, pp. 919–928, June 1999.
[4] P. Ciampolini, L. Roselli, G. Stopponi, and R. Sorrentino, "Global modeling strategies for the analysis of high-frequency integrated circuits," *IEEE Trans. Microwave Theory Tech.*, vol. 47, pp. 950–955, June 1999.
[5] M. A. Alsunaidi, S. M. Imtiaz, and S. M. El-Ghazaly, "Electromagnetic wave effects on microwave transistors using a full wave high-frequency time-domain model," *IEEE Trans. Microwave Theory Tech.*, vol. 44, pp. 799–808, June 1996.
[6] R. O. Grondin, S. M. El-Ghazaly, and S. Goodnick, "A review of global modeling of charge transport in semiconductors and full-wave electromagnetics," *IEEE Trans. Microwave Theory Tech.*, vol. 47, pp. 817–829, June 1999.
[7] S. G. Mallat, "A theory for multiresolution signal decomposition: The wavelet representation," *IEEE Trans. Pattern Anal. Mach. Intell.*, vol. 11, no. 7, pp. 674–693, July 1989.
[8] I. Daubechies, *Ten Lectures on Wavelets*. Philadelphia, PA: SIAM, 1992.
[9] I. McGarvey and E. Tentzeris, "Coupling of solid-state and electromagnetic equations," in *Proc. Eur. Microwave Conf.*, London, U.K., 2001.
[10] E. M. Tentzeris, A. Cangellaris, L. P. B. Katehi, and J. Harvey, "Multiresolution time-domain (MRTD) adaptive schemes using arbitrary resolutions of wavelets," *IEEE Trans. Microwave Theory Tech.*, vol. 50, pp. 501–516, Feb. 2002.
[11] M. Krumpholz and L. P. B. Katehi, "MRTD: New time-domain schemes based on multiresolution analysis," *IEEE Trans. Microwave Theory Tech.*, vol. 44, pp. 555–571, Apr. 1996.
[12] M. Werthen and I. Wolff, "A novel wavelet based time domain simulation approach," *IEEE Microwave Guided Wave Lett.*, vol. 6, pp. 438–440, Dec. 1996.
[13] M. Fujii and W. J. R. Hoefer, "A three-dimensional Haar-wavelet-based multiresolution analysis similar to the FDTD method—Derivation and application," *IEEE Trans. Microwave Theory Tech.*, vol. 46, pp. 2463–2475, Dec. 1998.
[14] S. Grivet-Talocia, "On the accuracy of Haar-based multiresolution time-domain schemes," *IEEE Microwave Guided Wave Lett.*, vol. 10, pp. 397–399, Oct. 2000.
[15] T. Dogaru and L. Carin, "Scattering analysis by multiresolution time domain method using compactly supported wavelet systems," *IEEE Trans. Microwave Theory Tech.*, vol. 50, pp. 1752–1760, July 2002.
[16] G. Carat *et al.*, "An efficient analysis of planar microwave circuits using a DWT-based Haar MRTD scheme," *IEEE Trans. Microwave Theory Tech.*, vol. 48, pp. 2261–2270, Dec. 2000.
[17] M. Fujii and W. Hoefer, "Field singularity correction in 2-D time-domain Haar-wavelet modeling of waveguide components," *IEEE Trans. Microwave Theory Tech.*, vol. 49, pp. 685–691, Apr. 2001.
[18] T. Dogaru and L. Carin, "Multiresolution time-domain using CDF biorthogonal wavelets," *IEEE Trans. Microwave Theory Tech.*, vol. 49, pp. 902–912, May 2001.
[19] C. Sarris and L. Katehi, "Fundamental gridding-related dispersion effects in multiresolution time-domain schemes," *IEEE Trans. Microwave Theory Tech.*, vol. 49, pp. 2248–2257, Dec. 2001.
[20] M. Fujii and W. Hoefer, "Time-domain wavelet-Galerkin modeling of two-dimensional electrically large dielectric waveguides," *IEEE Trans. Microwave Theory Tech.*, vol. 49, pp. 886–892, May 2001.
[21] J. Keiser, "Wavelet based approach to numerical solution of non-linear partial differential equation," Ph.D. dissertation, Univ. Colorado, Boulder, CO, 1995.
[22] M. Holmstron, "Solving hyperbolic PDE's using interpolating wavelets," Uppsala Univ., Uppsala, Sweden, Tech. Rep. 189/1996, 1996.
[23] S. Goasguen and S. M. El-Ghazaly, "Interpolating wavelet scheme toward global modeling of microwave circuits," in *IEEE MTT-S Int. Microwave Symp. Dig.*, 2000, pp. 375–378.
[24] S. Goasguen, M. M. Tomeh, and S. M. El-Ghazaly, "Interpolating wavelet scheme toward global modeling of microwave circuits," in *IEEE MTT-S Int. Microwave Symp. Dig.*, 2001, pp. 415–418.
[25] M. Toupikov, G. Pan, and B. K. Gilbert, "On nonlinear modeling of microwave devices using interpolating wavelets," *IEEE Trans. Microwave Theory Tech.*, vol. 48, pp. 500–509, Apr. 2000.
[26] Y. K. Feng and A. Hints, "Simulation of submicrometer GaAs MESFET's using a full hydrodynamic model," *IEEE Trans. Electron Devices*, vol. 35, pp. 1419–1431, Sept. 1988.
[27] P. Flandrin, *Time-Frequency/Time-Scale Analysis*. San Diego, CA: Academic, 1998.
[28] B. Hubbard, *The World According to Wavelets: The Story of a Mathematical Technique in the Making*. Wellesley, MA: A. K. Peters, 1998.
[29] B. Hilsum, "Simple empirical relationship between mobility and carrier concentrations," *Electron Lett.*, vol. 10, no. 12, pp. 259–260, 1974.

Yasser A. Hussein was born in Cairo, Egypt. He received the B.S. and M.S. degrees in electrical engineering from Cairo University, Cairo, Egypt, in 1995 and 1998, respectively, and is currently working toward the Ph.D. degree in electrical engineering at Arizona State University (ASU), Tempe.

His current research interests are in the areas of computer-aided design of microwave integrated circuits, computational electromagnetics and semiconductors, high-frequency RF modeling, genetic algorithms, wavelets, and wireless communications.

Samir M. El-Ghazaly (S'84–M'86–SM'91–F'01) received the Ph.D. degree in electrical engineering from the University of Texas at Austin, in 1988.

In August 1988, he joined Arizona State University, and became a Professor in 1998. He is currently the Department Head of Electrical and Computer Engineering, University of Tennessee, Knoxville. He has visited and worked at several universities and research centers including Cairo University, Cairo, Egypt, the Centre Hyperfrequences et Semiconducteurs, Université de Lille I, Lille, France, the University of Ottawa, Ottawa, ON, Canada, the University of Texas at Austin, NASA's Jet Propulsion Laboratory, Pasadena, CA, CST-Motorola Inc., Tempe, AZ, Institut d'Electronique de Microélectronique et de Nanotechnologie (IEMN), Université de Lille, and the Swiss Federal Research Institute (ETH), Zurich, Switzerland. His research interests include RF and microwave circuits and components, microwave and millimeter-wave semiconductor devices, semiconductor device simulations, ultrashort pulse propagation, microwave-optical interactions, linear and nonlinear modeling of superconductor microwave lines, wave–device interactions, electromagnetics, and numerical techniques applied to MMICs.

Dr. El-Ghazaly is a member of Tau Beta Pi, Sigma Xi, and Eta Kappa Nu. He is an elected member of Commissions A and D, URSI. He was the secretary and vice chairman, and is currently the chairman of Commission A, U.S. National Committee of URSI. He is a member of the Technical Program Committee for the IEEE Microwave Theory and Techniques Society (IEEE MTT-S) International Microwave Symposium (IMS) since 1991. He is on the Editorial Board of the IEEE TRANSACTIONS ON MICROWAVE THEORY AND TECHNIQUES. He was the chairman of the IEEE Waves and Devices Group, Phoenix Section. He was the chapter funding coordinator and chairman of the Chapter Activities Committee of the IEEE MTT-S. He is an elected member of the Administrative Committee of the IEEE MTT-S. He is the editor-in-chief of the IEEE MICROWAVE AND WIRELESS COMPONENTS LETTERS. He was the general chairman of the IEEE MTT-S 2001 IMS, Phoenix, AZ, May 2001.